Journal of Zhejiang University-SCIENCE C (Computers & Electronics)
ISSN 1869-1951 (Print); ISSN 1869-196X (Online)
www.zju.edu.cn/jzus; www.springerlink.com
E-mail: jzus@zju.edu.cn

High quality multi-focus polychromatic composite image fusion algorithm based on filtering in frequency domain and synthesis in space domain

Lei ZHANG, Peng LIU, Yu-ling LIU, Fei-hong YU[†‡]

(*State Key Lab of Modern Optical Instrumentation, Department of Optical Engineering, Zhejiang University, Hangzhou 310027, China*)

[†]E-mail: feihong@zju.edu.cn

Received June 8, 2009; Revision accepted Aug. 11, 2009; Crosschecked Mar. 29, 2010

Abstract: A novel multi-focus polychromatic image fusion algorithm based on filtering in the frequency domain using fast Fourier transform (FFT) and synthesis in the space domain (FFDSSD) is presented in this paper. First, the original multi-focus images are transformed into their frequency data by FFT for easy and accurate clarity determination. Then a Gaussian low-pass filter is used to filter the high frequency information corresponding to the image saliencies. After an inverse FFT, the filtered images are obtained. The deviation between the filtered images and the original ones, representing the clarity of the image, is used to select the pixels from the multi-focus images to reconstruct a completely focused image. These operations in space domain preserve the original information as much as possible and are relatively insensitive to misregistration scenarios with respect to transform domain methods. The polychromatic noise is well considered and successfully avoided while the information in different chromatic channels is preserved. A natural, nice-looking fused microscopic image for human visual evaluations is obtained in a dedicated experiment. The experimental results indicate that the proposed algorithm has a good performance in objective quality metrics and runtime efficiency.

Key words: Multi-focus image, Polychromatic image, Image fusion, Fast Fourier transform (FFT)
doi:10.1631/jzus.C0910344 **Document code:** A **CLC number:** TP391.41

1 Introduction

Because of the limited depth of focus (DOF) of an optical system, it is impossible to obtain an image with all information of a scene, especially when observing a 3D object or a thick specimen with a long focal length optical system. However, multi-focus images with complementary information of the observed object can be produced by moving the object along the optical axis. Increased confidence, reduced ambiguity, improved reliability, and improved classification can be achieved through image fusion. Human visual perception and computer-processing tasks such as segmentation, feature extraction, and object recognition will be made much easier with the fused image (Li *et al*., 2001). Images can be sharpened and certain features in either of the single data alone are extracted and enhanced (Yang *et al*., 2000). It can also be used in digital camera design or industrial inspection applications. If the focal length for each image is known, the decision map also determines a depth map that can be used for 3D surface reconstruction and 3D measurement (Sroubek *et al*., 2005). Many DOF extension algorithms exist to solve this problem. One of these methods is a wavefront coding system (Liu *et al*., 2008), which encodes the phase of the optical system with a phase mask on the pupil, and then decodes the acquired image to obtain the result for a large DOF. The image fusion is another important approach to extend the DOF (Yang *et al*., 2000; Li *et al*., 2001; Forster *et al*., 2004;

‡ Corresponding author

Sroubek *et al*., 2005; Zhao *et al*., 2008), which extracts details from multi-focus images to reconstruct the completely focused image. Because of the complexity of the wavefront coding system and the immaturity of the decoding algorithm, the multi-focus image fusion algorithm is still the most widely used method for extending the DOF.

The goal of the image fusion is to obtain an image with as many details from the multi-focus ones as possible. There are two main categories for this kind of algorithm: space domain and transform domain (such as the Fourier frequency domain and the multi-resolution pyramid decomposition domain). In the space domain, many focus measurement algorithms are employed as the focus degree assessment of the pixels, such as energy of image gradient (Huang and Jing, 2007), spatial frequency (Eskicioglu and Fisher, 1995), sum-modified-Laplacian, and high order statistics (Zhao *et al*., 2008). The pixels with the best focus degree are selected as the pixels of the fused image. In the multi-resolution pyramid decomposition domain, images are transformed into some coefficients which are combined with certain rules and then transformed back to get the fused image. Actually, the key point is the manipulation of the coefficients in the transform domain. The Laplacian pyramid (Burt and Andelson, 1983), the gradient pyramid (Burt *et al*., 1993), the ratio-of-low-pass pyramid (Toet *et al*., 1989), and the morphological pyramid (Matsopoulos *et al*., 1994) are examples of this kind of algorithm. Discrete wavelet transform (DWT) is another decomposition algorithm. In general, DWT is superior to the previous pyramid-based methods (Li *et al*., 1995; Pajares and Cruz, 2004). Localization can be preserved in both frequency and space domains (Yang *et al*., 2000). Complex wavelet transform (CWT) adds robustness to the selection rule and consistency check (Forster *et al*., 2004). However, the original pixel values of input images are not preserved in the fused image because wavelet transform methods directly apply the fusion rule to the coefficients in the transformed domain (Gabarda and Cristóbal, 2005). The proposed FFDSSD algorithm combines the advantages of space domain and transform domain, and the original pixel values are preserved, which makes it outperform the pure single domain methods.

Normally the following criteria should be considered when designing an image fusion algorithm (Oliver, 1996):

1. All relevant information of the input images should be preserved in the fused image.

2. Irrelevant information or noise should be suppressed.

3. Artifacts or inconsistencies that will affect further processing tasks should be avoided.

Experimental results show that the FFDSSD algorithm does well in all the aspects of the above criteria.

2 Multi-focus polychromatic image fusion with filtering in Fourier frequency domain and synthesis in space domain

2.1 Algorithm description

The key of the multi-focus image fusion is the determination of the focused regions of the images which will be extracted and then synthesized as the fusion result. For a partly focused image, the focused regions have more saliencies, so the Fourier spectrum of these regions definitely contains rich high-frequency components. On the other hand, the Fourier spectrum of the defocused regions contains fewer high-frequency components. As a result, Fourier spectrum can help distinguish the focused regions of the images. First, FFT is applied to a partly focused image:

$$F_{\text{freq}} = \Im\{\boldsymbol{I}\}. \tag{1}$$

Second, the transformed spectrum is filtered by a low-pass filter:

$$F_{\text{filtered}} = F_{\text{lp}} \times F_{\text{freq}}. \tag{2}$$

Third, the filtered spectrum is transformed back to the space domain:

$$\boldsymbol{I}_{\text{filtered}} = \Im^{-1}\{F_{\text{filtered}}\}. \tag{3}$$

In Eqs. (1)–(3), $\boldsymbol{I}$ stands for the original image, $\Im$ stands for the FFT, F_{freq} stands for the Fourier spectrum of the image, F_{lp} stands for the low-pass filter, $\Im^{-1}$ stands for the inverse FFT, and $\boldsymbol{I}_{\text{filtered}}$ stands for the filtered image.

After the transform-filter-inverse transform process, the original focused regions turn to blurred as a result of the low-pass filter, while the original blurred regions change little. Thus, the original and the transformed images can be compared to determine which regions contain more saliencies and which contain less. Then a difference matrix can be obtained by subtracting the original image from the transformed one. For convenience, the difference matrix should be non-negative so that the larger the value of the matrix element, the clearer the corresponding image pixel. Therefore, the absolute value of each element in the difference matrix is calculated as

$$\boldsymbol{E}_{\text{diff}} = \left| \boldsymbol{I} - \boldsymbol{I}_{\text{filtered}} \right|, \tag{4}$$

where $\boldsymbol{E}_{\text{diff}}$ is the difference matrix.

Each image in the multi-focus images corresponds to a difference matrix and the pixels with the maximum value in the difference matrix are selected as the object pixels (maximum selection):

$$\boldsymbol{I}_d(m,n) = \boldsymbol{I}^i(m,n), \quad \text{if} \quad \boldsymbol{E}^i_{\text{diff}}(m,n) > \boldsymbol{E}^j_{\text{diff}}(m,n), \tag{5}$$

where m is the row index, n is the column index, $\boldsymbol{I}_d$ is the fused image, P is the number of the multi-focus images, i, j=1, 2, ..., P and $i \neq j$, $\boldsymbol{I}^i$ is the ith image in the image sequence, and $\boldsymbol{E}^i_{\text{diff}}$ is the corresponding difference matrix of the ith image.

The fusion scheme is shown in Fig. 1, in which the fusion process of the proposed algorithm is clearly depicted. For each image, a difference matrix needs to be calculated according to Eq. (4), which means that there are as many difference matrices as the images to be fused. The fusion of the images is the selection of the pixels from the original multi-focus images according to the comparison result of the difference matrices.

2.2 Noise handling

If the maximum selection strategy is adopted as the fusion rule, one pixel in the fused image comes from a pixel of one image in the original multi-focus images. If one of the multi-focus images contains noise, its Fourier spectrum will contain rich high-frequency components. Consequently, the pixels in it are quite possible to be selected as the object pixels. However, if the weighted average method is adopted as the fusion rule, each pixel in the original images will contribute to the fused image and the noise contained in one of the source images will decrease due to the weighted average. The elements of the difference matrix are considered as weights, and the fused image is the weighted average of the original multi-focus images (weighted average):

$$\boldsymbol{I}^{\text{noise}}_d(m,n) = \frac{\sum_{i=1}^{p} \boldsymbol{I}^i(m,n)\boldsymbol{E}^i_{\text{diff}}(m,n)}{\sum_{i=1}^{p} \boldsymbol{E}^i_{\text{diff}}(m,n)}, \tag{6}$$

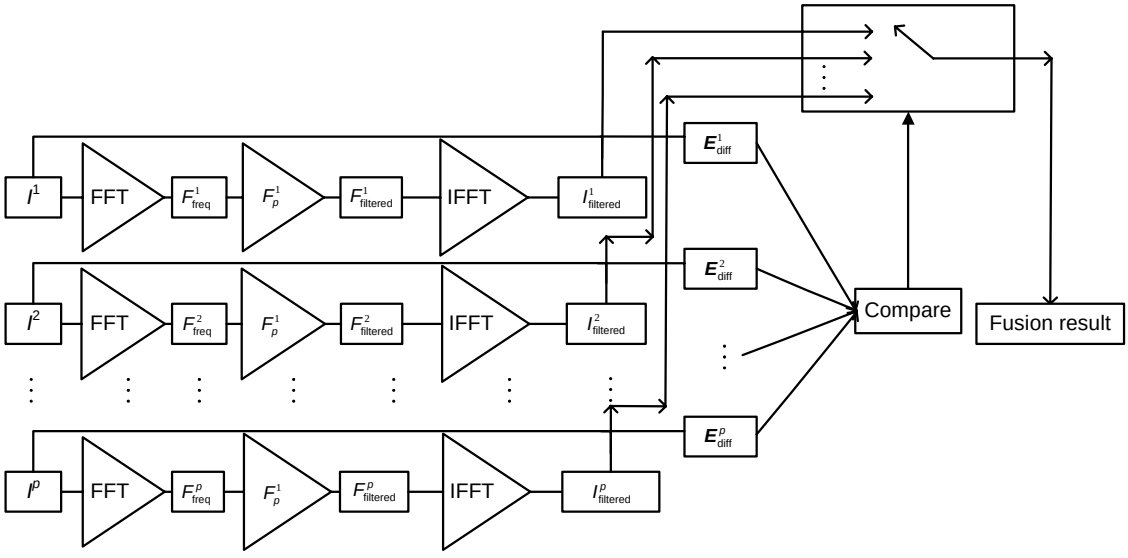

Fig. 1 Schematic diagram of filtering in frequency domain and synthesis in space domain (FFDSSD)

where $\boldsymbol{I}_d^{\text{noise}}$ is the fused image of the multi-focus images with one noise-added image.

On the other hand, the decrease of the noise is accompanied by the loss of the image contrast. Therefore, images with and without noise should be treated separately.

2.3 Polychromatic channels handling

Polychromatic noise will be introduced into the fused image if different chromatic channels are not properly treated. This will greatly affect the human visual inspection. If different chromatic channels of a pixel in the fused image come from different images of the original multi-focus images, a great deal of chromatic noise will appear in the fused image. In this paper, the following scheme is applied to handle this problem. The images are first converted from RGB to YCbCr color space and the Y (luminance) channel is used to calculate the difference matrices. Then the pixels of the fused image are selected from the original images in RGB space according to the difference matrices calculated in Y. Human vision has different responses to difference colors. In YCbCr color space saliencies contained in different RGB channels will be treated differently according to their RGB color channels, which is consistent with the human vision characteristic.

The operation is described as follows: (1) For each image, convert the image to YCbCr color space; (2) Calculate the difference matrix $\boldsymbol{E}_{\text{diff}}$ with the Y channel; (3) Select one entire pixel from the original images according to $\boldsymbol{E}_{\text{diff}}$.

2.4 Low-pass filter design

As discussed above, a proper low-pass filter is also an essential part of the proposed algorithm. The following are principles for the design of the low-pass filter:

1. A smooth profile across the whole frequency band.

2. A moderate attenuation in the high frequency band, and the attenuation decreases with the decrease of the frequency. Therefore, different frequency components have different attenuations.

3. The second derivative of the profile along the radial direction should be negative so that the variety of the profile is large enough, which ensures that different levels of details could be easily distinguished.

4. Normalized to 1.

In the second principle, it is pointed out that the attenuation decreases with the decrease of the frequency and different frequency components should have different attenuations. This is because different kinds of images have different Fourier spectral distributions and if two bands of the Fourier spectrum have the same attenuation, it will be difficult to tell which regions are clearer, for the regions containing the two bands of spectral components will possibly have the same difference matrix element values.

The Gaussian filter is adopted in the experiment. According to the theory of the proposed algorithm, it is insensitive to the filter parameters as long as the above requirements are met. For convenience, the variance is half length of the diagonal line of the image:

$$\sigma = \sqrt{M^2 + N^2}/2, \tag{7}$$

$$F_{\text{G}}(m,n) = \exp\left(-(m^2+n^2)/(2\sigma^2)\right), \tag{8}$$

$$F_{\text{lp}}(m,n) = F_{\text{G}}(m,n)/\max\{F_{\text{G}}(m,n)\}, \tag{9}$$

where M and N stand for the width and height of the image respectively, and F_{lp} stands for the low-pass filter.

2.5 Algorithm performance for misregistration scenarios

According to Section 2.1, the selection of the focused regions depends on the degree of the image degradation after the transform-filter-inverse transform process. That is, the focused regions still possess a larger value of the difference matrix elements than the defocused regions at the same pixel positions located on the other images. Therefore, the fusion result could still contain the focused regions, although there are offsets to their original positions. The image contrast is not decreased and all the useful features are preserved. However, in transform domain methods, original images are decomposed into some coefficients that are used to fuse the images. Misregistration will lead to a lower contrast due to the coefficients of the focused and defocused regions which are directly manipulated by fusion rules in the process, such as the weighted average and maximum/minimum selection. Experiments in Section 3.4 will show this.

3 Experimental results and algorithm comparison

The following four multi-focus images captured with an automatized microscope are used to illustrate the proposed algorithm. From Figs. 2a–2d, each image in the image sequence contains both focused regions and defocused regions. The focused regions, which contain the characteristics of an insect, move from the bottom to the top from Figs. 2a–2d and it can be clearly seen that each figure contains different focused and defocused regions.

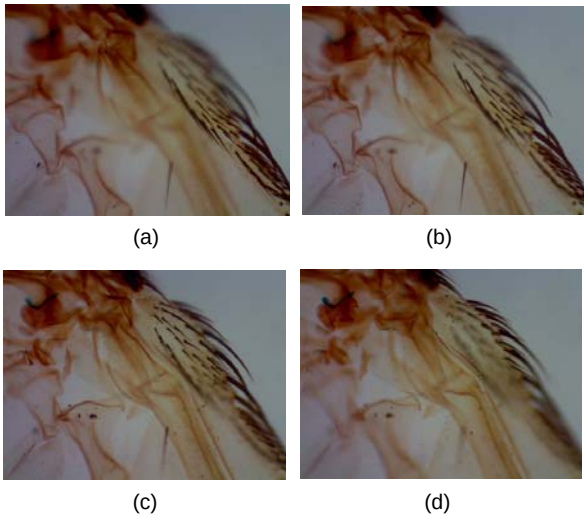

Fig. 2 Multi-focus images used for experiment
(a) Focuses on bottom-right; (b) Focuses on middle-bottom; (c) Focuses on middle-top; (d) Focuses on top-right

Visual inspection gives a direct assessment but it is easily influenced by visual and psychological factors. Therefore, the quality assessment of the fused image should also be based on objective quantitative evaluation criteria. For multi-focus images, it is impossible to get the ground truth image as a reference, so the quality metrics such as the root mean square error (RMSE) and the peak signal-to-noise ratio (PSNR) are not adopted. In order to give an objective quality assessment for the proposed algorithm, standard deviation (STD), information entropy (IE), variance, energy of Laplacian (EOL), spatial frequency (SF) (Huang and Jing, 2007), and similarity (De and Chanda, 2006) are adopted as the quality metrics. The polychromatic images are converted to gray level images to compute the quality metric indices.

3.1 Sensitivity to the Gaussian low-pass filter parameter σ

The following are fusion results of different Gaussian low-pass filter parameters and the corresponding filter profiles. The dimension of the image is 400×300. It can be seen that the fusion quality is increasing from Figs. 3a, 3c to 3e. There are obvious artifacts in Fig. 3a, and the contrast of the setae of the insect is low. The reason is that the Gaussian filter parameter is too small for the profile of the filter to meet the second principle in Section 2.4:

1. The attenuation in the high frequency band is too high (actually zero).

2. Across a large frequency band, there is no attenuation change, resulting in failure to distinguish different levels of details.

For Fig. 3c, the image quality is fairly well but not as good as Fig. 3e. The variety of the filter is not so large because the second derivative in the high frequency band is positive. As a result, the deviations between the original images and the processed images are not prominent, which conflicts with the third principle in Section 2.4.

From Table 1, it can be seen that the fusion result with σ=250 outperforms the others for most of the quality metrics. But for EOL and SF, the values are lower than the others. That is because artifacts are introduced with an improper σ, which is considered by these metrics as details. For statistical quality metrics, the artifacts do not contribute to the fusion result for they are actually noise.

Table 1 Performance of different Gaussian filter parameter σ's

σ	STD	IE	Variance	EOL	SF	Similarity
50	10.8424	6.5774	916.2195	1.1381E9	11.6236	0.5647
100	10.7807	6.5870	946.2044	1.1713E9	12.1782	0.5897
250	11.0478	6.5980	988.7927	1.0218E9	12.0631	0.5959

STD: standard deviation; IE: information entropy; EOL: energy of Laplacian; SF: spatial frequency

According to our experiments, the choosing of the parameter σ is arbitrary as long as the principles in Section 2.4 are met. The half length of the diagonal line is a useful selection (actually a value which is a little smaller or larger will not noticeably affect the quality of the fusion result). However, if the parameters of the images change, there is no need to

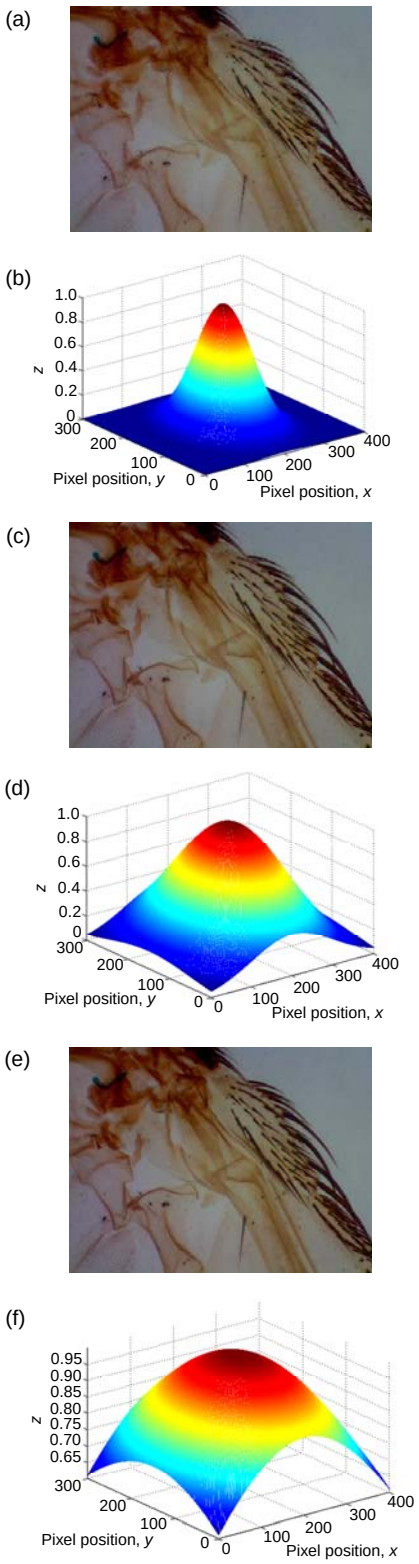

Fig. 3 Performance of different Gaussian filter parameter σ's. (a), (c), and (e) are fusion results of σ=50, 100, and 250, respectively; (b), (d), and (f) are low-pass filter of σ=50, 100, and 250, respectively

manually select another parameter, such as the image block size, threshold, wavelet base, and decomposition level, for the FFDSSD. This makes the proposed algorithm more universal.

3.2 Performance compared with DWT and CWT

The traditional DWT and CWT are selected here as the target algorithms for comparison. For both DWT and CWT, each image is decomposed into wavelet subbands. After all the multi-focus images are decomposed, the maximum absolute value selection fusion rule is applied to the subbands. That is, the wavelet coefficients with the largest absolute value are selected as the fused coefficients. Then, the fused coefficients are transformed back. For DWT, the fusion result is the inverse transformation result, while for CWT the fusion result is the real part of the inverse transformation (Forster *et al*., 2004). The fusion result of the proposed algorithm is shown in Fig. 4c and the DWT and CWT results are respectively shown in Figs. 4a and 4b for a comparison.

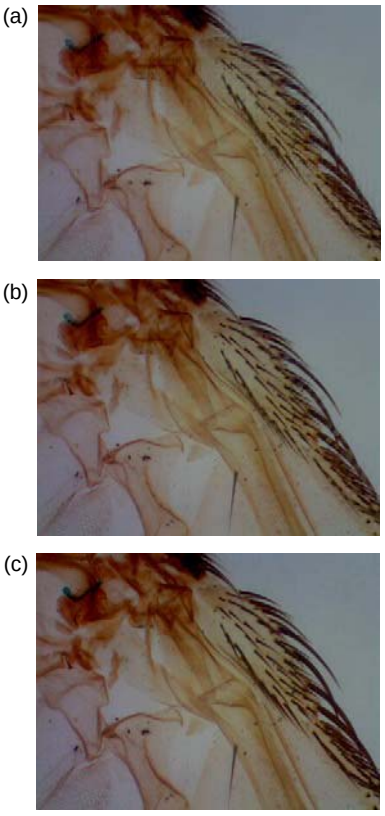

Fig. 4 Fusion results of different algorithms. (a) DWT (db3, level 3); (b) CWT (complex db3, level 3); (c) FFDSSD

In Fig. 4c, it can be seen that most of the saliency information contained in the original multi-focus images is preserved in the result image after the fusion process and few artifacts or noise is introduced. The setae of the insect, which are important to distinguish the species of the insect, are very clear in the fused image. Fig. 4a is the fusion result of DWT, and obvious zigzag artifacts can be found near the edge of the setae in the image. In Fig. 4b, the contrast of the image is reduced and there are periodic artifacts on the setae of the insect. It is obvious that the proposed algorithm outperforms DWT and CWT in visual inspection. Image quality metrics shown in Table 2 indicate that the FFDSSD outperforms DWT and CWT on objective criteria.

Table 2 Performance of different algorithms for images in Fig. 2

Algorithm	STD	IE	Variance	EOL	SF	Similarity
FFDSSD	11.0478	6.5980	988.7927	1.0218E9	12.0631	0.5959
DWT	10.6512	6.5524	865.0870	0.4762E9	9.0108	0.5327
CWT	10.7930	6.5268	854.6706	0.7693E9	10.6521	0.5666

STD: standard deviation; IE: information entropy; EOL: energy of Laplacian; SF: spatial frequency; FFDSSD: filtering in the frequency domain and synthesis in the space domain; DWT: discrete wavelet transform; CWT: complex wavelet transform

3.3 Performance for the noise-added image

In order to find out whether the proposed algorithm is noise insensitive or not, one image in Fig. 2 is added Gaussian noise with a variance of 0.005. For simplicity, Fig. 2a is replaced by the noise-added image shown in Fig. 5.

Fig. 5 Image with 0.005 variance Gaussian noise

Comparing Fig. 6c with Fig. 4c, the contrast of the weighted average result is not as high as the maximum selection, but the noise contained in one of the original images is suppressed, especially on the setae of the insect and no obvious artifacts are introduced, although there is still noise on the background. Since the background regions contain few high frequency components, the weights of these regions are very low and the weighted average scheme could not solve this problem. For the fusion result of DWT and CWT in Figs. 6a and 6b, the zigzag and periodic artifacts still exist and there is some noise on the setae of the insect. The image quality metrics of fusion results for images with noise are shown in Table 3.

(a)

(b)

(c)

Fig. 6 Fusion results of different algorithms for images with noise

(a) DWT (db3, level 3); (b) CWT (complex db3, level 3); (c) FFDSSD

Table 3 Performance of different algorithms for images with noise

Algorithm	STD	IE	Variance	EOL	SF	Similarity
FFDSSD	10.4814	6.8424	961.5944	6.6533E9	22.6178	0.5715
DWT	10.6057	6.8231	957.5947	6.4637E9	22.4794	0.5695
CWT	10.5441	6.8248	932.3269	7.3921E9	24.0826	0.5897

STD: standard deviation; IE: information entropy; EOL: energy of Laplacian; SF: spatial frequency; FFDSSD: filtering in the frequency domain and synthesis in the space domain; DWT: discrete wavelet transform; CWT: complex wavelet transform

3.4 Performance for the misregistration scenario

To test the sensitivity of the proposed algorithm to the misregistration issue, the images in Fig. 2 are manually given as two pixels offset to the left, top, right, and bottom, respectively. The offset images are shown in Fig. 7.

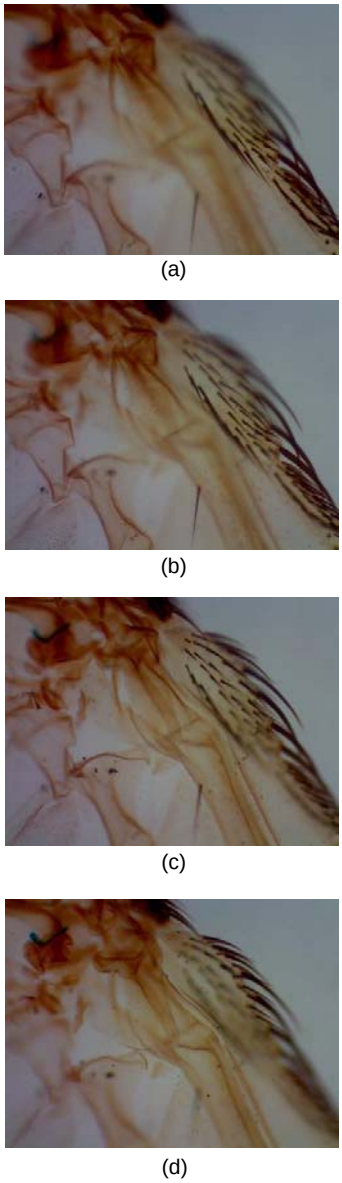

(a)

(b)

(c)

(d)

Fig. 7 Unregistered multi-focus images used for experiment

(a) Two pixels to the left; (b) Two pixels to the top; (c) Two pixels to the right; (d) Two pixels to the bottom

It can be clearly seen that the zigzag artifact is even worse in Fig. 8a compared with Fig. 4a. The contrast of the CWT result is still reduced and the periodic artifact is even more distinct. Although there is a little offset for the FFDSSD result, the features of the original unregistered images are extracted into the fusion result. The useful information is preserved in the fusion process, and the quality metrics in Table 4 also show this.

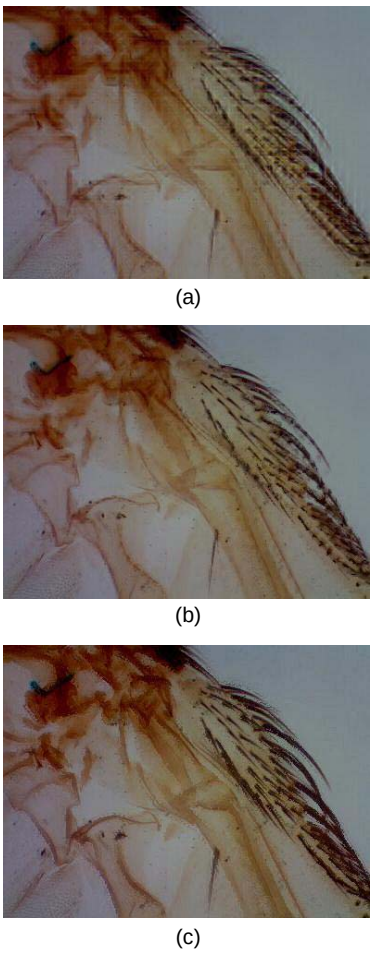

(a)

(b)

(c)

Fig. 8 Fusion results of the unregistered images

(a) DWT (db3, level 3); (b) CWT (db3, level 3); (c) FFDSSD

Table 4 Performance of different algorithms for unregistered images

Algorithm	STD	IE	Variance	EOL	SF	Similarity
FFDSSD	10.9511	6.6370	1009.5000	2.4849E9	15.9017	0.5914
DWT	10.6189	6.5807	854.7185	0.5925E9	9.6649	0.5274
CWT	10.4733	6.4947	789.7812	0.8482E9	10.7670	0.5408

STD: standard deviation; IE: information entropy; EOL: energy of Laplacian; SF: spatial frequency; FFDSSD: filtering in the frequency domain and synthesis in the space domain; DWT: discrete wavelet transform; CWT: complex wavelet transform

3.5 Run-time efficiency

For an image of $n \times n$ dimension, the computational complexity of FFT is $n^2 \log n$, while for DWT, the computational complexity is $n^3 \log n$ (Helmy and Sam, 2003). It is obvious that the FFDSSD will run faster than the wavelet approach under the same hardware and software circumstance.

The algorithms are implemented on a laptop of Intel Core Duo Mobile Processor T8100 and 4 GB DDR2 667 MHz memory with Matlab 7.7. The average time consumption is shown in Table 5. It can be seen that the proposed algorithm is much more efficient than the wavelet algorithms. With proper optimization of the code, such as implementing the algorithm with a more efficient programming language and fully utilizing the hardware instructions of a particular computer structure, the FFDSSD can run real time in outdoor environments on a laptop without requiring too much hardware resource.

Table 5 Performance of different algorithms for unregistered images

Image (pixels)	Time consumption (s)		
	FFDSSD	DWT	CWT
400×300	0.9046	5.6916	6.3615
1600×1200	14.2260	95.7299	142.3319

FFDSSD: filtering in the frequency domain and synthesis in the space domain; DWT: discrete wavelet transform; CWT: complex wavelet transform

4 Conclusion

A novel multi-focus polychromatic image fusion algorithm based on filtering in the frequency domain and synthesis in the space domain is presented in this paper. Experimental results are described in detail. The proposed algorithm performs well in the following aspects: (1) the fused image has a good visual effect and contains few artifacts; (2) the proposed algorithm is relatively noise and misregistration insensitive; (3) there are no additional parameters that are needed to be changed with different kinds of images, i.e., block size, threshold, wavelet base, and decomposition level; (4) the proposed algorithm has a relatively high computational efficiency. Despite the fact that the multi-focus images are used in the experiment, the proposed algorithm can be easily extended for dealing with arbitrary images with spatial-variant (Rajagopalan and Chaudhuri, 1997) blur, such as atmospheric turbulence. This algorithm has been successfully implemented in ScopePhoto (ScopeTek, http://www.scopetek.com), which is widely used in the digital microscopes for the thick specimen or for the sample which cannot be cut into thin slices. Feedbacks show a great success of the application. The height information can also be extracted from the difference matrices during selecting the maximum value of the matrices. Thus, the proposed algorithm can also be used to extract 3D information of real objects, which will be useful in metallographic analysis for metal defect detection, biomedical analysis for disease diagnosis, cell recognition and 3D measurement. Future work will be related to the extension of the algorithm to other areas such as multi-sensor image processing and so on. System-on-chip (SOC) implementations of image processing algorithms are going to become more common in the near future. We believe our method will promisingly be useful in this aspect.

Acknowledgements

We would like to thank the financial support from the Hangzhou ScopeTek Opto-Electric Co., Ltd. With this support, we have the high quality instruments to setup our experiment to implement our algorithm.

References

Burt, P., Andelson, E.H., 1983. The Laplacian pyramid as a compact image code. *IEEE Trans. Commun.*, **31**(4):532-540. [doi:10.1109/TCOM.1983.1095851]

Burt, P., Hanna, K., Lolczynski, R., 1993. Enhanced Image Capture through Fusion. Proc. 4th Int. Conf. on Computer Vision, p.173-182. [doi:10.1109/ICCV.1993.378222]

De, I., Chanda, B., 2006. A simple and efficient algorithm for multifocus image fusion using morphological wavelets. *Signal Process.*, **86**(5):924-936. [doi:10.1016/j.sigpro.2005.06.015]

Eskicioglu, A., Fisher, P., 1995. Image quality measures and their performance. *IEEE Trans. Commun.*, **43**(12):2959-2965. [doi:10.1109/26.477498]

Forster, B., van de Ville, D., Berent, J., Sage, D., Unser, M., 2004. Complex wavelets for extended depth-of-field: a new method for the fusion of multichannel microscopy images. *Microsc. Res. Techn.*, **65**(1-2):33-42. [doi:10.1002/jemt.20092]

Gabarda, S., Cristóbal, G., 2005. On the use of a joint spatial-frequency representation for the fusion of multi-focus images. *Pattern Recogn. Lett.*, **26**(16):2572-2578. [doi:10.1016/j.patrec.2005.06.003]

Helmy, A.E., Sam, K., 2003. A computationally efficient algorithm for multifocus image reconstruction. *SPIE*, **5017**:332-341. [doi:10.1117/12.476754]

Huang, W., Jing, Z., 2007. Multi-focus image fusion using pulse coupled neural network. *Pattern Recogn. Lett.*, **28**(9):1123-1132. [doi:10.1016/j.patrec.2007.01.013]

Li, H., Manjunath, B., Mitra, S., 1995. Multi-sensor image fusion using the wavelet transform. *Graph. Models Image Process.*, **57**(3):235-245. [doi:10.1006/gmip.1995.1022]

Li, S., James, T.K., Wang, Y., 2001. Combination of images with diverse focuses using the spatial frequency. *Inf. Fus.*, **2**(3):169-176. [doi:10.1016/S1566-2535(01)00038-0]

Liu, Q., Zhao, T., Zhang, W., Yu, F., 2008. Image restoration based on generalized minimal residual methods with antireflective boundary conditions in a wavefront coding system. *Opt. Eng.*, **47**(12):127005. [doi:10.1117/1.3050348]

Matsopoulos, G., Marshall, S., Brunt, J., 1994. Multiresolution morphological fusion of MR and CT images of the human brain. *IEE Proc.-Vis. Image Signal Process.*, **141**(3):137-142. [doi:10.1049/ip-vis:19941184]

Oliver, R., 1996. Pixel-Level Fusion of Image Sequences Using Wavelet Frames. Proc. 16th Leeds Applied Research Workshop, p.149-154.

Pajares, G., Cruz, J., 2004. A wavelet-based image fusion tutorial. *Pattern Recogn.*, **37**(9):1855-1872. [doi:10.1016/j.patcog.2004.03.010]

Rajagopalan, A.N., Chaudhuri, S., 1997. Space-variant approaches to recovery of depth from defocused images. *Comput. Vis. Image Underst.*, **68**(3):309-329. [doi:10.1006/cviu.1997.0534]

Sroubek, F., Gabarda, S., Redondo, R., Fischer, S., Cristobal, G., 2005. Multifocus fusion with oriented windows. *SPIE*, **5839**:264-273. [doi:10.1117/12.608399]

Toet, A., Valeton, J., van Ruyven, L., 1989. Merging thermal and visual images by a contrast pyramid. *Opt. Eng.*, **28**(7):789-792. [doi:10.1117/12.55479]

Yang, X., Yang, W., Pei, J., 2000. Different Focus Points Images Fusion Based on Wavelet Decomposition. Proc. 3rd Int. Conf. on Information Fusion, MOD3/3-8.

Zhao, H., Li, Q., Feng, H., 2008. Multi-focus color image fusion in the HIS space using the sum-modified-Laplacian and a coarse edge map. *Image Vis. Comput.*, **26**(9):1285-1295. [doi:10.1016/j.imavis.2008.03.007]